Wideband Terahertz Band Reflection and Diffuse Scattering Measurements for Beyond 5G Indoor Wireless Networks

Joonas Kokkoniemi*, Vitaly Petrov†, Dmitri Moltchanov†,
Janne Lehtomäki*, Yevgeni Koucheryavy†, and Markku Juntti*
*Centre for Wireless Communications (CWC), University of Oulu, P.O. Box 4500, 90014 Oulu, Finland,
Email: joonas.kokkoniemi@ee.oulu.fi, janne.lehtomaki@ee.oulu.fi, markku.juntti@oulu.fi.
†Department of Electronics and Communications Engineering, Tampere University of Technology, 33720 Tampere, Finland
Email: vitaly.petrov@tut.fi, dmitri.moltchanov@tut.fi, yk@cs.tut.fi

***Abstract*—Measurement results on rough surface scattering on common indoor materials in the terahertz (THz) band from 100 GHz to 4 THz are reported. The measurements were made using THz time domain spectroscopy (THz-TDS)-based measurement device in multiple transmitter and receiver angles for five different materials: aluminium, glass, plastic, hardboard, and concrete. The main interest of this paper is in the frequency domain characteristics of the scattering and reflections on different materials from the viewpoint of possible non-line-of-sight (NLOS) communications in the THz band. The measurements show that the specular reflection component always dominates, even in the case of rather rough concrete sample. The main reason for this is the vast bandwidth: the lower frequencies tend to have strong specular component even if the higher frequencies would diffuse on surface of the material. The results also show that the diffuse scattering field is very weak in comparison to the specular direction. However, it is still theoretically high enough to enable the NLOS links on short distances. The results clearly show that the NLOS paths, especially, reflected paths, can be used for communications in the THz band.**

I. Introduction

Increasing demand for larger bandwidths for the future communication systems has turned the interest from the exhausted ultra high frequency band (UHF) of 0.3–3 GHz towards the higher frequencies. The upcoming 5G systems will utilize the extremely high frequency band (EHF) of 30–300 GHz, or more commonly, millimeter-waves (mmWaves) [1], [2]. These frequencies offer much more spectrum than any lower frequency band with the drawback of smaller communication radius. The small cell sizes, on the other hand, offer highly increased data rates due to smaller numbers of customers, thus, higher frequency reuse in small geographical coverage areas [1]. Taking the small cells to the extreme, the THz frequency band (0.1–10 THz) may just be the answer for the ultra high data rate communications at short distances [3], as the theoretical data rates rise up to several terabits per second even with the simple pulse based modulations [4]. The down side of the THz band is its very high path loss, which requires small cell sizes and preferably line-of-sight (LOS) between transmitter (Tx) and receiver (Rx).

The main difference of the THz band communications to, e.g., UHF band communications is the molecular absorption. The molecular absorption causes frequency selective fading to the signals as electromagnetic waves' energy is partially absorbed by the molecules in the air, most notably by the water vapor in the atmosphere [4]. The molecular absorption increases exponentially with distance between Tx and Rx. However, it is very predictable because of the vast number of molecules per unit volume of the atmosphere. There are many papers about modeling the molecular absorption with the help of databases [4]–[6], which can be used in the theoretical assessment of the strength of the absorption loss.

In this paper, we focus on the rough surface scattering measurements. Our main interest is in the frequency domain behavior of the reflected and scattered THz radiation. The non-LOS (NLOS) propagation phenomena, including the penetration, reflections, and scattering, are of particular interest for the computer simulation models for the THz communication systems. Ray tracing, for instance, can effectively be used to model a link between devices, or a network of devices, in realistic environments. This kind of a model requires information on the NLOS propagation phenomena to model the ray propagation on the objects in the communication medium properly. Another use case for the NLOS measurement result is to adjust/check validity of the theoretical models, which we will address in the future work.

Several studies provided empirical and theoretical rough surface scattering results for the THz band [7]–[14]. The majority of these papers focus on the lower part of the THz band, around 300 GHz. The main insight of those studies is that the specular component has the most power. Although the diffuse scattering did provide some contribution, its effect is significantly smaller than the reflected paths. This can also be

This work was supported by Infotech Oulu Doctoral Program, Academy of Finland SeCoFu project and Academy of Finland FiDiPro program "Nanocommunication Networks". The authors would also like to thank the following foundations for their support: Riitta ja Jorma J. Takasen säätiö, Walter Ahlströmin säätiö, Tauno Tönningin säätiö, Ulla Tuomisen säätiö, and Nokia Foundation.

ISBN 978-3-8007-4221-9

shown theoretically, which is briefly reviewed in Section II.

In this paper, our interest is in the THz band in general, at the limits of our measurement device, i.e., from approximately 0.1 to 4 THz. Having the indoor THz communications in mind, we report on measurements on common materials found in indoor locations including aluminium, glass, plastic, hardboard, and concrete. The Rx and Tx angles to the surface of the material were varied. To obtain deep insights on the scattering phenomenon we mainly focus on the frequency domain results. Indeed, the higher the frequency, the higher is the chance on the diffuse scattering dependent on the surface roughness. The results show the diffuse scattering field is very weak and mostly under the noise, but in some cases it is high enough to enable NLOS communications. On the other hand, the reflected components are rather strong and easily allow communication through reflected paths.

The main application for the reported results is link- and system-level analysis of THz communications using ray-tracing simulations in realistic indoor deployments. Ray-tracing models require detailed information on the radiation behavior on the objects and obstacles in the medium. Characterization of these objects requires empirical knowledge on the penetration and scattering properties of different surface materials. Extending this knowledge is our aim in this paper.

II. Rough Surface Scattering Theory

We briefly look into the rough surface scattering theory in this section. The theory is familiar from multiple rough surface scattering papers, such as [7]–[9], [13], [14]. The theoretical path gain $L(f, \sigma_h, l_c, \theta_1, \theta_2, \theta_3)$ for a rough surface with infinite conductivity is given by [7], [8]

$$L(f,\sigma_h, l_c, \theta_1, \theta_2, \theta_3) = e^g \left(\rho^2 + \frac{\pi l_c^2 F^2}{A} \sum_{m=1}^{\infty} \frac{g^m}{m! m} e^{-v_{xy}^2 l_c^2 / 4m} \right), \quad (1)$$

where

$$\rho = \mathrm{sinc}(v_x l_x)\mathrm{sinc}(v_y l_y), \quad (2)$$

$$v_x = k(\sin(\theta_1) - \sin(\theta_2)\cos(\theta_3)), \quad (3)$$

$$v_y = k(-\sin(\theta_2)\sin(\theta_3)), \quad (4)$$

$$v_{xy} = \sqrt{v_x^2 + v_y^2}, \quad (5)$$

$$F = \frac{1 + \cos(\theta_1)\cos(\theta_2) - \sin(\theta_1)\sin(\theta_2)\cos(\theta_3)}{\cos(\theta_1)(\cos(\theta_1) + \cos(\theta_2))}, \quad (6)$$

$$g = k^2 \sigma_h^2 (\cos(\theta_1) + \cos(\theta_2))^2, \quad (7)$$

where l_c is the surface correlation length, σ_h is the standard deviation of the surface height variations, θ_1 is the elevation of the incident radiation, θ_2 is the elevation of the scattered radiation, θ_3 is the azimuth of the scattered radiation, g is the Rayleigh roughness factor, ρ^2 is the specularly reflected component, l_x and l_y give the fractional area on the surface under investigation (the surface can be broken into a grid of areas $A = l_x l_y$, with $l_x, l_y \gg \lambda$, where λ is the wavelength

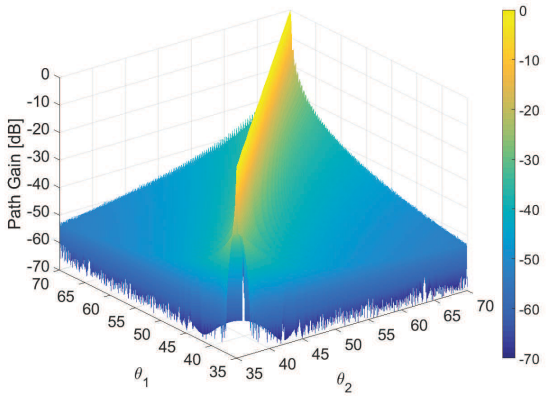

Fig. 1. A theoretical path gain at one THz as a function of θ_1 and θ_2.

[7]), and k is the angular wave number. More information on these parameters and the rough surface scattering theory can be found in the references [7]–[9], [13], [14].

Fig. 1 shows the path gain at one THz frequency as a function of elevation angles θ_1 and θ_2. The azimuth angle θ_3 is assumed to be zero. The area on the surface is assumed to be $l_x l_y = \pi$ with equal l_x and l_y, which is the approximate surface area of the THz beam. Furthermore, the surface correlation length is assumed to be $l_c = 0.01$ cm and surface height distribution $\sigma_c = 10^{-4}$ cm. Thus, the example surface is a very smooth with a high number of surface variations. We can see a very similar pattern to ones presented in the later on in the measurement results (Figs. 8 and 9). The main difference becomes from the fact that the measurements have a beam diameter of approximately two centimeters at the sample, which widens the specular response. Also, the exact surface properties are for our samples are unknown for now, as they require further investigation with electron microscope in the future to accurately predict the corresponding surface height distributions and correlation length. Despite the unknown parameters, the theory matches the measurement results relatively accurately, making the utilization of the above theory in the future perfectly possible in the case of wide band THz scattering measurements.

III. Measurement Setup

The measurement setup consisted of a THz band measurement device and a variety of different samples. The measurement device was TeraView TeraPulse 4000, which is based on terahertz time domain spectroscopy (THz-TDS), in which the full time domain detection window is composed of multiple short time duration windows, determining also the resolution time of the full time domain signal. The signal amplitude is detected one short time window at the time. By delaying the reception step-by-step, the full time domain signal can be captured. It was composed of 2000 samples with the resolution time of approximately 100 fs. Thus, the total detection window was 200 ps long. To decrease the noise level, all the results are based on an average of 50 individual measurements. Translating the above figures into frequency domain means 5 THz bandwidth with the frequency resolution

ISBN 978-3-8007-4221-9

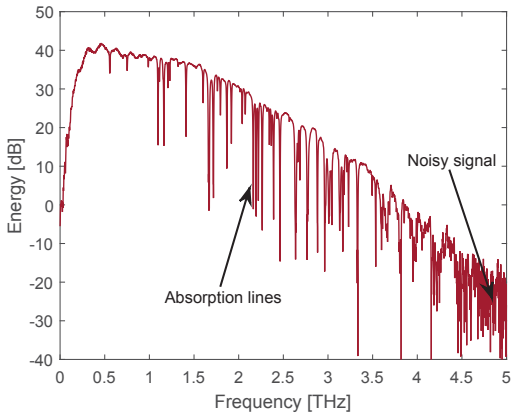

Fig. 2. The pulse shape of the TeraView TeraPulse in frequecy domain.

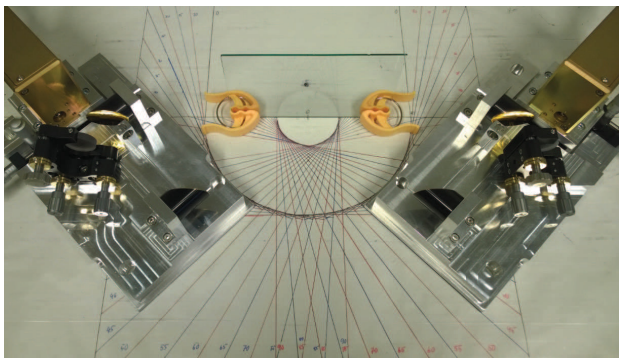

Fig. 3. The measurement setup showing the THz emitter and receiver heads, along with the optics and glass sample with the Tx and Rx in 45 degree angle to the sample.

of 5 GHz. However, in the results, we have used additional zero padding to increase the visual frequency resolution to approximately one GHz. Although the theoretical bandwidth is 5 THz, approximately 4 THz is usable because the signal is exponentially decaying towards the end of the frequency band of interest. After approximately 4 THz it is completely under the noise level, which has an impact on the accuracy of the results at the higher end of the measurement band. The pulse shape of TeraPulse in dB-scale is shown in Fig. 2.

Fig. 3 shows the measurement setup. The THz beam is directed with the optics to achieve nearly perfectly straight beam at the sample location. The samples were placed in the zero position between the measurement head plates and adjusted to be in perfect 90 degree angle in both horizontal and vertical directions. The total path length in all the cases is approximately 60 cm, of which 20 cm comes from the plate separation and about 2×20 cm from the optics. In Fig. 3, one can see the utilized glass sample in place with the both measurement heads at 45 degree angle to the sample. The angle of the both Tx and Rx was varied from 35 to 70 degrees. The angle is relative to the tangent of the surface. Any lower angle would have been not possible for all the samples since the device's beam width is approximately two centimeters. Thus, the whole THz beam would have not hit the surface at lower angles. The higher angles were, on the other hand,

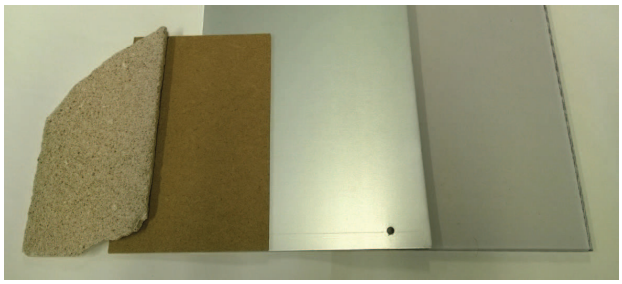

Fig. 4. The other samples besides the glass sample (visible in Fig. 3): concrete, hardboard, aluminium, and plastic, from left to right, respectively.

limited by the size of the measurement head plates. Higher (and also lower) angles would have been possible, but not for all the angle combinations.

The rest of the samples, besides the glass (visible in Fig. 3), are shown in Fig. 4. These samples were chosen because they are common in any indoor, or outdoor locations. They included aluminium, glass, plastic, hardboard, and concrete. Furthermore, these samples gave quite a good overview of the different roughnesses found in the indoor locations. The aluminium sample was moderately polished unfinished aluminium sheet with rather smooth surface. The glass sample was regular glass found, e.g., in windows. This was the smoothest sample among all the samples along with the plastic sample, which was chosen to be styrene-acrylonitrile sheet due to being common in plastic windows. The second roughest sample was hardboard, which is very common, e.g., in the structures of bookshelves. Because of being composed of the compressed wood fibres, it has relatively smooth surface with moderately rough finish. The concrete sample was by far the roughest sample among the considered ones. It had a straight face, but otherwise it was unpolished, non-coated concrete. These samples give already quite good overview of different materials and roughnesses that can be found in indoor and outdoor locations.

IV. Numerical Results

The frequency domain energies as a function of the receiver angle are given in Figs. 5 and 6 for aluminium and concrete, respectively. The Tx angle is fixed at 50 degrees. These samples were chosen for the figures, since they represent the two extremes of the measurements: aluminium was the strongest reflector and concrete was the strongest scatterer. The other samples more or less represent the aluminium response, with some differences as it can be seen in the case of the path gain figures below.

The aluminium gives a quite representative result on what was expected, and what was the general observation of the measurements: the largest contribution comes from the reflected path, with minor response at the diffuse scattering field. This is also true for the concrete. However, it gives far less energy at the reflected path, but also the most energy in the diffuse scattering directions. What can also be seen is that the lower frequencies contribute much more at higher angle offsets than the higher frequencies. The first reason is the scattering increases with frequency (see, e.g., [15]). Thus,

ISBN 978-3-8007-4221-9

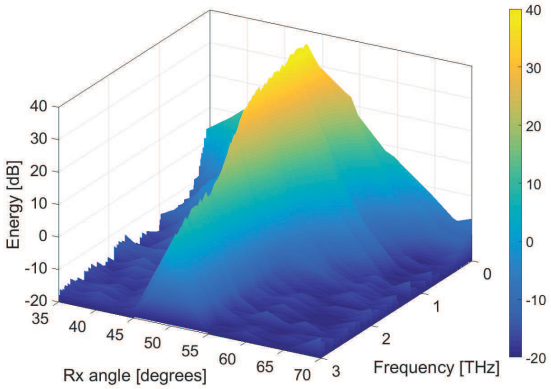

Fig. 5. The measured frequency responses for aluminium at the 50 degree Tx angle as a function of the receiver angle.

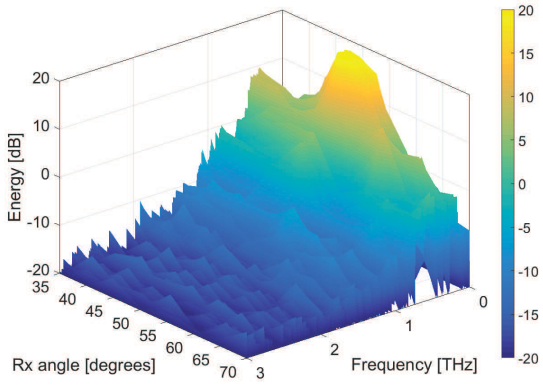

Fig. 6. The measured frequency responses for concrete at the 50 degree Tx angle as a function of the receiver angle.

the higher frequency components should have flatter response over the receiver angles. This leads as to the second reason: the frequency response would be lower in any case at the higher frequencies because of the signal shape. This causes the weak responses to be easily hidden by the noise. However, this is a very interesting result, as it shows the THz band encompasses both strong reflected components, as well as perceptible diffuse scattering field. Theoretically there is no reason why neither of these could be used for communications in the NLOS directions.

To estimate the relative strengths of the reflections and scattering, we rely on the path gain, which is obtained by screening the measurement results against direct path measurement. The straight path measurements were made at the same distance between the Tx and Rx plates as in the case of measurements on the samples, i.e., 20 cm separation between the measurement head platforms (visible in Fig. 3). The frequency domain path gain corresponds to the channel power transfer function:

$$\frac{S_{\mathrm{sc}}(f)}{S_{\mathrm{c}}(f)} = \frac{H_{\mathrm{sc}}(f)X(f)+N_{\mathrm{sc}}}{H_{\mathrm{c}}(f)X(f)+N_{\mathrm{c}}} = \frac{H_{\mathrm{s}}(f)H_{\mathrm{c}}(f)X(f)+N_{\mathrm{sc}}}{H_{\mathrm{c}}(f)X(f)+N_{\mathrm{c}}} \approx H_{\mathrm{s}}(f) + \frac{N_{\mathrm{sc}}}{H_{\mathrm{c}}(f)X(f)}, \tag{8}$$

where $S_{\mathrm{sc}}(f)$ is the received signal power through reflected/scattered path and channel, $S_{\mathrm{c}}(f)$ is the straight reference signal power, i.e., the straight path measurement, $H_{\mathrm{sc}}(f)$ is the channel power transfer function of the reflected/scattered path and channel, $H_{\mathrm{c}}(f)$ is the power transfer function of reference channel, N_{sc} is the noise in the measurement of a sample, N_{c} is the noise of the reference measurement, $X(f)$ is the unknown signal power envelope, and $H_{\mathrm{s}}(f)$ is the pure reflection/scattering power transfer function. In the case of the last noise term, we assume the noise power N_{c} is small in comparison to the reference signal power (see, e.g., Fig. 2) as a consequence of the full LOS path having significantly more power in comparison to the reflected/scattered paths. This causes a noise coloring in the reflection/scttering path gains. Therefore, this last term causes the false path gain increase in the higher frequencies. In reality, the path gain decreases towards zero according to the contour of the smooth part of the path gain. The point where the noise component starts to significantly affect the results (and render them unreliable) is easy to see due to the random white noise-like fluctuations from the 2nd term in (8) as opposed to smooth behavior of the 1st term in (8).

Figs. 7(a) to 7(d) illustrate the path gains of the considered materials at fixed Tx angle of 35 degrees at the Rx angles 35, 40, 50, and 65 degrees, respectively. The first two angles have either full, or partial visibility of the Tx at Rx through the reflected paths, whereas the last two figures depict a situation in diffuse scattering field only. Note the sharp spiked features in the responses are caused by the molecular absorption: where the reference signal goes near the noise level, there are sharp spikes after division. Some spikes are partially caused by division with close to zero value, but also because of a slight mismatch between absorption features between reference and the sample measurements. The THz band is sensitive to the humidity changes because of the absorption of energy in the water molecules. The first figure (Fig. 7(a)) shows the reflection properties up to 4 THz due to the reflected path gives relatively much energy even at the higher frequencies. The rest of the figures are cut from the 2 THz as consequence of the desired signal going under the noise power.

We can see some interesting features in these figures: aluminium is the strongest reflector, but not on all the frequencies. The glass and the plastic partially exceed the aluminium's response between 1.5 and 2 THz. The reason for this is most likely the very smooth surface of the glass and plastic in comparison to the aluminium. The aluminium seems to have strong diffuse scattering between 1.5 and 2.5 THz, because an absorption on the non-coated aluminium is unlikely. This can be caused, e.g., by the refractive index causing weaker reflections at certain frequencies. The refractive index is both frequency dependent, and linked with the reflectivity of the material [16, Chapter 35.4]. Still, the overall energy advantage goes to the aluminium because it does not allow any penetration, whereas the glass and plastic do.

ISBN 978-3-8007-4221-9

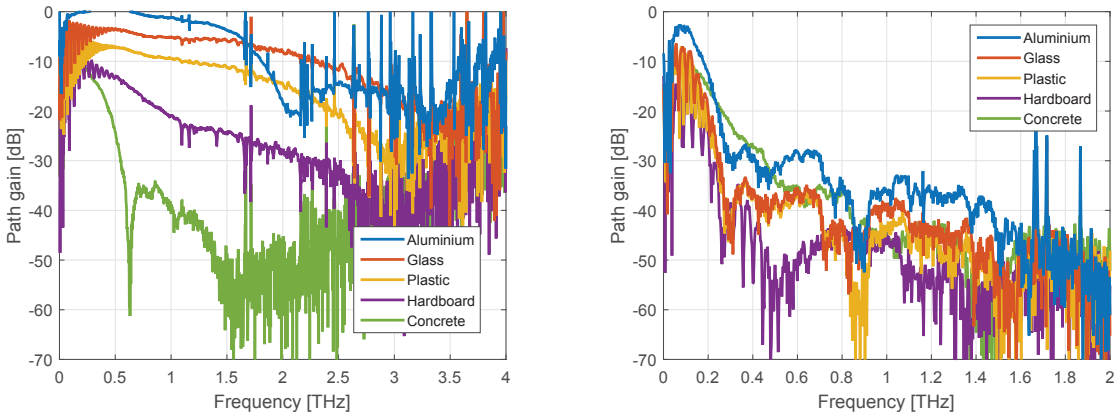

(a) Rx angle 35 degree.

(b) Rx angle 40 degree.

(c) Rx angle 50 degree.

(d) Rx angle 65 degree.

Fig. 7. The path gains of the materials as a function of frequency. The Tx angle was fixed at 35 degrees and the Rx angle was 35, 40, 50, and 65 degrees in Figs. 7(a), 7(b), 7(c), and 7(d), respectively.

As soon as the reflected components are lost, the concrete is the only significant contributor to the energy. Because the signal has a shape below 0.1 THz, the results are not reliable below this limit. The path loss is very high, but given a short enough distance, communication solely through the diffuse scattering field is theoretically possible. On the other hand, communication through reflected paths is very plausible due to path gain varying between 0 and -20 dB below 2.5 THz for aluminium, glass, and plastic, and being at somewhat tolerable level on the other two materials also. As it can be seen in Fig. 7(d), as well as in Fig. 6, very rough surfaces may cause some problems even in the reflected paths, but especially below 0.5 THz the losses are small enough to ensure tolerable path loss.

To show some general path gain figures, Figs. 8 and 9 show the total path gains for glass and hardboard as a function of Rx and Tx angles. The path gains in these figures were calculated as ratios between the scattering/reflection energies and the reference measurement energy, integrated over all frequencies. These figures mainly continue to give the same statement of the previous discussion: the reflected path gives the most energy, whereas outside the specular field the response quickly drops. We can see the glass gives slightly wider response, which is a direct consequence of the discussion above: the glass reflects better than the hardboard, thus, also retaining the energy better in the specular field than the hardboard. If we had plotted similar figures for all the materials, we would have seen nearly identical figures, even in the case of concrete because the total energy is dominated by the low frequency specular components. The main differences between the materials would have been at the specular components. The information on these can be seen in Figs. 7(a) to 7(d).

V. Discussion

We presented the results of the rough surface measurement campaign focusing on the common materials found in the indoor locations. The measurements showed the reflected components offer quite reasonable response, with some materials almost acting as mirrors at some frequencies (within the measurement error), e.g., the aluminium below one THz. The same can be expected on all the metals because of the in general poor penetrability of electromagnetic waves to the metals. For the same reason the measurement devices optics are gold plated: efficient reflectivity. Whereas plastics offer rather good penetration at the THz band, smoothness also

ISBN 978-3-8007-4221-9

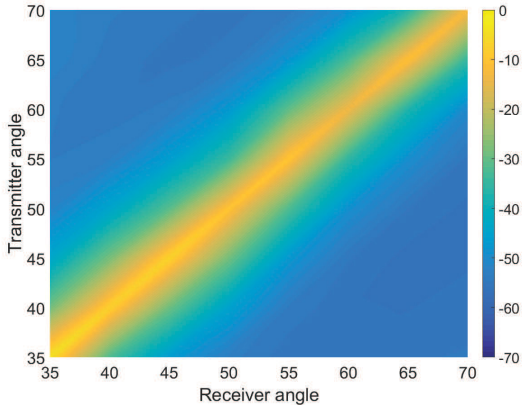

Fig. 8. The path gains for glass as a function of transmitter and receiver angles

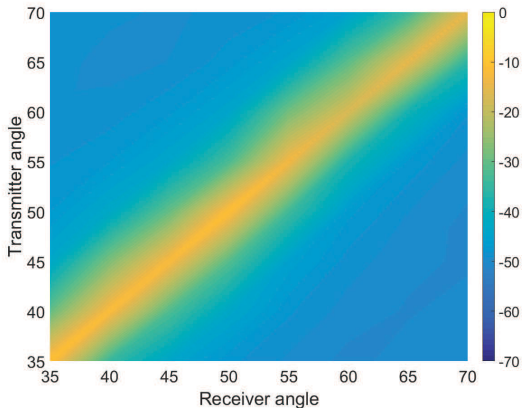

Fig. 9. The path gains for hardboard as a function of transmitter and receiver angles.

allows high reflectivity. Actually, all the materials here allowed high enough reflections to allow communication in the NLOS paths. The diffuse scattering response also existed for all the materials. However, to get a good contribution from the non-specular directions, relatively rough surface is required, as the concrete in our case. The overall picture of the results indicate a strong possibility to communicate through the reflected paths, as well the diffuse scattering field to some extent. The future work on the surface scattering includes an investigation of the surface properties of the real materials in order to utilize the corresponding rough surface theories.

The measurement device has a very directional beam. This is a good property, as the realistic high frequency links will most likely be very directional to mitigate the large path loss. The narrow links require highly directional reception, which also makes the initial signal search difficult. On the other hand, the reasonable reflection loss in the channel does not necessarily require LOS, but the NLOS paths can also be utilized in the communications. Since there are possibly many paths from the Rx to Tx, the reflected path can theoretically be used in the signal establishment, while searching for the strongest path later in the communication process.

The observation on the existence of the potential NLOS paths is very important for the link and the network simulations focusing on, e.g., the above mentioned signal search and communication via the NLOS paths. For instance, geometrical propagation simulation models, i.e., the ray tracing models, require information on the material reflectivities in order to properly model response of the Tx, or the entire network at the Rx. While it is interesting to know the reflections and scattering do show contribution in the THz band, it also makes things complicated for the simulation models. The reflections, scattering, and possible penetration losses need to be taken into account in the simulations. Neglecting these effects may cause too optimistic simulation or theoretical results, whether we talk about enhanced energy at the reception of the desired symbol, or interference on the subsequent symbols, or undesired links. On the other hand, as mentioned above, the NLOS path can be the life line in signal search, or the entire link in the absence of LOS path.

REFERENCES

[1] T. S. Rappaport *et al.*, "Millimeter wave mobile communications for 5G cellular: It will work!" *IEEE Access*, vol. 1, no. 1, pp. 335–349, May 2013.

[2] A. L. Swindlehurst, E. Ayanoglu, P. Heydari, and F. Capolino, "Millimeter-wave massive mimo: The next wireless revolution?" *IEEE Commun. Mag.*, vol. 52, no. 9, pp. 56–62, Sep. 2014.

[3] I. F. Akyildiz, J. M. Jornet, and C. Han, "Terahertz band: Next frontier for wireless communications," *Phys. Commun.*, vol. 12, pp. 16–32, Sep. 2014.

[4] J. M. Jornet and I. F. Akyildiz, "Channel modeling and capacity analysis for electromagentic nanonetworks in the terahertz band," *IEEE Trans. Wireless Commun.*, vol. 10, no. 10, pp. 3211–3221, Oct. 2011.

[5] S. Paine, "The *am* atmospheric model," Smithsonian Astrophysical Observatory, Tech. Rep. 152, 2012.

[6] L. S. Rothman *et al.*, "The HITRAN 2008 molecular spectroscopic database," *J. Quant. Spectrosc. Radiat. Transfer*, vol. 110, no. 9–10, pp. 533–572, Jun.–Jul. 2009.

[7] C. Jansen, S. Priebe, C. Möller, M. Jacob, H. Dierke, M. Koch, and T. Kürner, "Diffuse scattering from rough surfaces in THz communication channels," *IEEE Trans. THz Sci. Technol.*, vol. 1, no. 2, pp. 462–472, Nov. 2011.

[8] S. Priebe, M. Jacob, C. Jansen, and T. Kürner, "Non-specular scattering modeling for THz propagation simulations," in *IEEE European Conf. Antennas Propag.*, 2011, pp. 1–5.

[9] R. Piesiewicz, C. Jansen, D. Mittleman, T. Kleine-Ostmann, M. Koch, and T. Kürner, "Scattering analysis for the modeling of thz communication systems," *IEEE Trans. Antennas Propag.*, vol. 55, no. 11, pp. 3002–3009, Nov. 2007.

[10] R. Piesiewicz, M. Jacob, M. Koch, J. Schoebel, and T. Kürner, "Performance analysis of future multigigabit wireless communication systems at thz frequencies with highly directive antennas in realistic indoor environments," *IEEE J. Sel. Topics Quantum Electron.*, vol. 14, no. 2, pp. 421–430, Mar. 2008.

[11] S. Priebe, C. Jastrow, M. Jacob, T. Kleine-Ostmann, T. Schrader, and T. Kürner, "Channel and propagation measurements at 300 ghz," *IEEE Trans. Antennas Propag.*, vol. 59, no. 5, pp. 1688–1698, May 2011.

[12] R. Piesiewicz, T. Kleine-Ostmann, N. Krumbholz, D.Mittleman, M. Koch, and T. Kürner, "Terahertz characterisation of building materials," *IEEE Electron. Lett.*, vol. 41, no. 18, pp. 1002–1004, Sep. 2005.

[13] C. Han, A. O. Bicen, and I. F. Akyildiz, "Multi-ray channel modeling and wideband characterization for wireless communications in the terahertz band," *IEEE Trans. Wireless Commun.*, vol. 14, no. 5, pp. 2402–2412, May 2015.

[14] A. Moldovan, M. A. Ruder, I. F. Akyildiz, and W. H. Gerstacker, "LOS and NLOS channel modeling for terahertz wireless communication with scattered rays," in *Globecom Workshops*, 2014, pp. 388 – 392.

[15] J. Kokkoniemi, J. Lehtomäki, and M. Juntti, "Frequency domain scattering loss in THz band," in *Proc. Global Symb. Milli. Waves*, 2015, pp. 1–3.

[16] H. D. Young and R. A. Freedman, *Sears and Zemansky's University Physics: with Modern Physics (11th ed.)*, A. Black, Ed. Addison Wesley, 2003.

ISBN 978-3-8007-4221-9